JOURNAL OF GEOPHYSICAL RESEARCH, VOL. 101, NO. B6, PAGES 13,805–13,817, JUNE 10, 1996

Scaled experiments of volcanic spreading

Olivier Merle
Département des Sciences de la Terre, Université Blaise Pascal, Clermont-Ferrand, France

Andrea Borgia
Instituto Nazionale di Geofisica, Rome, Italy

Abstract. Experiments were conducted to study the spreading of volcanic constructs. Volcanoes are simulated by a sand cone, and the volcanic substratum is simulated by a sand layer (brittle substratum) overlying a silicone layer (ductile substratum). Similarity conditions between natural volcanoes and experimental prototypes led to the definition of dimensionless Π numbers. Experiments determine Π values which predict whether or not spreading takes place. Of particular importance are the ratio between the thickness of the brittle substratum and the height of the volcano (Π_2) and the brittle/ductile ratio of the substratum (Π_3). Π_2 indicates that the volcano must be large enough to "break" the substratum before spreading occurs, whereas Π_3 controls the style of deformation. During spreading, these dimensionless numbers change with time, reaching values that tend toward those observed for stable configurations. Experimental values are compared with those from well-constrained natural examples. It is found that an essential requirement for volcanic spreading is the presence of a low-viscosity layer within the substratum. Flow of the weak layer away from the excess load is responsible for the spreading. The overlying edifice displays radial intersecting grabens, due to concentric stretching, dissected summit areas; concentric zones of thrusts and folds form in the substratum around the edifice, and diapirs of the ductile substratum rise within the fault zones.

Introduction

The process of volcanic spreading is now being recognized as one of the most relevant in controlling the slow-rate long-term structural and magmatic evolution of volcanic edifices [cf. *Delaney,* 1992; *Kerr*, 1994; *Borgia*, 1994]. A volcano of sufficient size induces stresses that may deform its substratum; in turn, this deformation feeds back stresses which deform the edifice; both stresses and deformation influence the evolution of magma by varying the boundary conditions of magmatic systems.

In order of increasing size, volcanic spreading is inferred to be active at Concepcion Volcano in Nicaragua [*van Wyk de Vries et al.*, 1993], Poàs Volcano in Costa Rica [*Borgia et al.*, 1990], various volcanoes of Sumatra and Java [*van Bemellen*, 1956], Etna Volcano in Italy [*Borgia et al.*, 1992], Marsili Seamount in the Thyrrenian Basin [*Argnani et al.*, 1993], the Cappadocia Volcanic Complex in Turkey [*Pasquarè et al.*, 1993], the Mauna Loa-Kilauea Volcanic system [*Borgia* 1990, 1994; *Borgia and Treves*, 1992; *Clague and Denlinger*, 1994], and the Olympus Mons on Mars [*Borgia et al.*, 1990]. Some of these authors show that thin-skinned shortening, due to folding and thrusting, around the base of these volcanoes is compensated by sagging of the edifices and summit extension. A weak basal layer decouples the deformation of the volcano and of its immediate substratum from that of the crust.

Borgia [1994] used numerical analyses to show that two elements of volcanoes are of particular importance in driving the process: (1) the weight of the edifice onto the substratum and (2) the long-term deformation of the intrusive complexes. In this work, we use three-dimensional (3-D) scale experiments to study the influence of the first of these elements on the structural evolution of volcanoes.

Our experiments do not model the effect of the intrusive complexes; they cannot be used as exact scale analogs of volcanoes where the intrusive complexes give the dominant contribution to deformation, such as the Mauna Loa-Kilauea system [*Borgia*, 1994] or the Cappadocia Volcanic complex [*Pasquarè et al.*, 1993]. Experiments to model this contribution are presented by *Merle et al.* [1993] and *Merle and Vendeville* [1995]. In addition, our experiments do not model the effect of subsidence due to crustal flexure under the load of volcanic edifices. This effect is especially important for large fast growing volcanoes such as hot spot volcanoes [*McGovern and Solomon,* 1993; *Borgia*, 1994].

Paper number 95JB03736.
0148-0227/96/95JB-03736$09.00

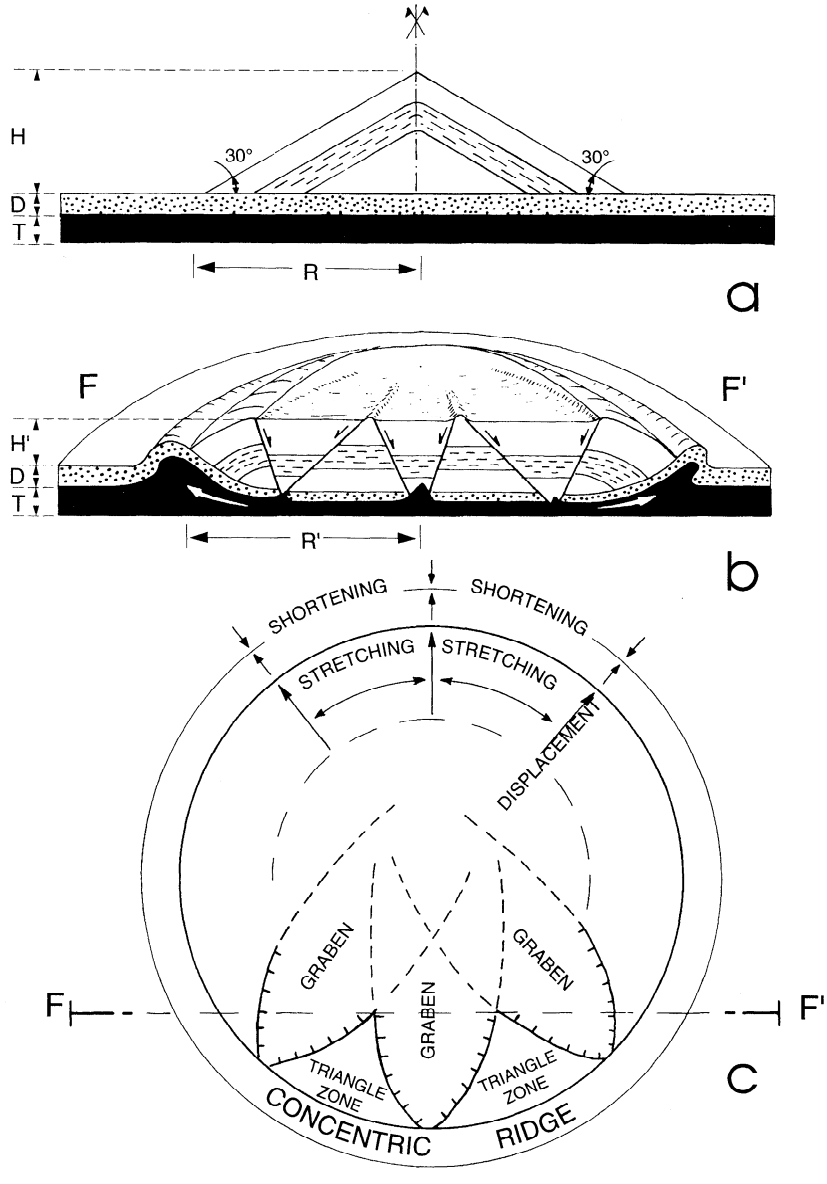

Figure 1. Schematic representation of the volcanic spreading process as shown from experiments. (a) Cross section of the initial stage. (b) Cross section after deformation showing the flow of the weak layer (in black), the folding and faulting the volcano, and the horst and graben structures within the volcano. (c) Top view after deformation showing the relationship between structures (grabens and triangular horsts and a concentric ridge) and the strain pattern associated with the spreading process (radial displacement, concentric stretching in the volcano, and radial shortening in the substratum surrounding the volcano).

In these experiments, we consider the volcanic edifice as being cooled, and we do not take into account any contribution of magma forces to the destabilisation process. Even though these approximations may appear to be an oversimplification of reality, we show that complex structures develop within and around the volcano and that these structures can be identified both in the field and in remote sensing images.

Scaling

The scale model of the volcano is intended to be geometrically, kinematically and dynamically similar to natural volcanoes. We use the standard similarity conditions as explained, for instance, by *Hubbert* [1937] and *Ramberg* [1981]. The model volcano (Figure 1) consists of a cone constructed by pouring dry sand onto a substratum. Since we want to investigate the effect of the load of the volcano only, the cone has no viscous or ductile core. The substratum is a brittle upper layer, dry sand, and a weak lower layer, viscous silicone.

Principal geometric variables (Figure 1 and Table 1) are the height (H) and radius (R) of the sand cone, and the depth to (D) and the thickness of (T) the weak lower layer. Of course, D is also the thickness of the sand layer in the substratum. Material property variables are the densities of

Table 1. Average Geometric and Mechanical Variables in Real and Analogue Volcanoes

Variable	Definition	Value		Dimensions
		Field	Experiment[a]	
H	thickness of volcanic cone	$1.2\text{-}3.0\times10^{3}$	$5\times10^{-2}\rightarrow2.3\times10^{-2}$	m
R	radius of volcanic cone	$5\text{-}20\times10^{3}$	$8.5\times10^{-2}\rightarrow12.5\times10^{-2}$	m
D	thickness of brittle substratum	$0\text{-}10^{3}$	$5\times10^{-3}\rightarrow5\times10^{-3}$	m
T	thickness of weak substratum	$10^{2}\text{-}10^{3}$	$5\times10^{-3}\rightarrow2.5\times10^{-3}$	m
ρ_v	density of volcanic cone	$2.5\text{-}2.8\times10^{3}$	1.4×10^{3}	kg m^{-3}
ρ_s	density of substratum	$2.0\text{-}2.5\times10^{3}$	1.4×10^{3}	kg m^{-3}
t	time span for deformation	10^{12}	3.5×10^{4}	s
μ	viscosity of weak substratum	10^{17}	2×10^{4}	Pa s
Φ	angle of internal friction	30°	30°	
g	gravity acceleration	9.8	9.8	m s^{-2}

[a] The experimental values are measured at the start and end of the experiments of figures 2c-2d.

the sand volcano (ρ_v) and of the substratum (ρ_s), the angle of internal friction of the brittle material (Φ), and the viscosity (μ) of the weak layer (Table 1). The only force is gravity (g). The time span in which most of the deformation takes place is t.

Therefore according to the Buckingham-Π theorem, there are 10 variables minus 3 dimensions equal to 7 independent dimensionless numbers (Table 2) that need to maintain the same value between the field and the experimental systems to guarantee similarity.

Of these, three numbers are obviously the geometric ratios of the system:

$$\Pi_1 = \frac{height\ of\ volcano}{radius\ of\ volcano} = \frac{H}{R}, \quad (1)$$

$$\Pi_2 = \frac{thickness\ of\ brittle\ layer}{height\ of\ volcano} = \frac{D}{H}, \quad (2)$$

$$\Pi_3 = \frac{thickness\ of\ brittle\ layer}{thickness\ of\ weak\ layer} = \frac{D}{T}. \quad (3)$$

One other dimensionless number must be related to the difference in density between the volcano and its substratum:

$$\Pi_4 = \frac{density\ of\ volcano}{density\ of\ substratum} = \frac{\rho_v}{\rho_s}. \quad (4)$$

Gravity is balanced in the sand by forces that resist failure, in the silicone by inertial and viscous forces. Thus, the other three dimensionless numbers should be ratios of these forces. Observing that a reasonable scaling parameter for the velocity of the process could be the ratio between the thickness of the weak layer and the time span in which most of the deformation occurs (T/t), these numbers are

$$\Pi_5 = \frac{gravitational\ force}{viscous\ force} = \frac{\rho_v g H t}{\mu}, \quad (5)$$

$$\Pi_6 = \frac{failure\ resistance\ force}{viscous\ force} = \frac{2\tan\Phi\rho_v g(H+D)t}{3\mu} + \tan\Phi,$$

$$= \tan\Phi\left(\frac{2}{3}\Pi_5(1+\Pi_2)+1\right) \quad (6)$$

Table 2. Average Π Dimensionless Numbers in the Field and Experiments

Dimensionless Variable	Definition	Value	
		Field	Experiment
Π_1	height/radius of volcano	0.15-0.2	0.58→0.18
Π_2	brittle substratum/height of volcano	0-1.5	0.1→0.22
Π_3	brittle/weak substratum	0-15	1→2
Π_4	volcano/substratum density	1-1.4	1
Π_5	gravitational/ viscous forces	790	1200
Π_6	frictional/ viscous forces	82-327	160
Π_7	inertial/viscous forces	10^{20}	10^{12}

$$\Pi_7 = \frac{inertial\ force}{viscous\ force} = \frac{\rho_s T^2}{\mu t} \quad (7)$$

which is the Reynolds number. In (5)-(7) the gravity, inertial, and viscous forces per unit area scale respectively as

$$gravitational\ force = \rho_r g H , \quad (8)$$

$$inertial\ force = \frac{\rho_s (T/t)^2}{T} = \frac{\rho_s T}{t^2} , \quad (9)$$

$$viscous\ force = \frac{\mu (T/t)}{T} = \frac{\mu}{t} . \quad (10)$$

The failure resistance force per unit area (failure stress, τ) is estimated via the Coulomb-Navier failure criterion with no cohesion [*Hubbert and Rubey*, 1959]:

$$\tau = \tan\Phi(\sigma_1 - \sigma_3) , \quad (11)$$

where σ_1 and σ_3 are the maximum and minimum principal stresses given by

$$\sigma_1 = \rho_r g(H+D) \quad (12)$$

and since σ_3 is equal to the stress due to volcanic loading plus the stress due to viscous deformation,

$$\sigma_3 = \frac{1}{3}\rho_r g(H+D) - \frac{\mu}{t} . \quad (13)$$

The geometric ratios used in our experiments (Tables 1 and 2) have values that model real volcanoes that are 1-3 km high and 5-20 km in radius ($\Pi_1 \approx 0.15$-0.2). They overlie a substratum with a weak layer at depths ranging from 0 to 1500 m ($\Pi_2 \approx 0$-1.5) and 100 to 1000 m in thickness ($\Pi_3 = 0.1$-15).

In nature, Π_4 is on average larger than 1. Thus, in some experiments, cast-iron powder is added to the sand to increase the density of the volcano prototype with respect to that of the substratum. As will be described in the following section, this ratio influences the complexity and the rate of deformation of the system, but it does not affect significantly the type of deformation.

The ratios of gravity to viscous forces, Π_5, and of frictional to viscous forces, Π_6, cannot be neglected, and they must maintain values in the experiment as close as possible to the real ones. However, from the definition of Π_6 given in (7) we observe that this number can be expressed as a function of Π_5, Π_2, and Φ. Thus this condition is implicitly satisfied once the other quantities are equal.

Finally, the very small value of Π_7 (10^{-20}, Table 2) indicates that in nature, inertial forces are negligible with respect to viscous forces. In our experiments, Π_7 is about 10^{12} (Table 2) and cannot reach the extremely low natural values. In fact, even using materials of very unusual properties, for instance, of high viscosity ($\mu > 10^6$ Pa s) and low density ($\rho_s < 10^2$ kg m^3), and an extremely thin weak layer in the substratum ($T < 10^{-3}$ m), it would be difficult to achieve values of Π_7 smaller than 10^{-16}, because the experiments will last for too long a time span ($t > 10^6$ s). Still, to a very good approximation, the inertial forces are negligible with respect to the viscous forces. Thus this number may receive no further consideration. Accordingly, to maintain similarity only the first five numbers need to have experimental values close to those of real volcanoes (Table 2).

Materials of the Experiments

We use dry sand as an analog for brittle rocks. The sand is a cohesionless granular material that fails according to the Navier-Coulomb criterion of brittle failure. The angle of friction Φ is about 30°. It is considered a good analog for brittle rocks and has been used as such in many previous experiments [e.g., *Faugère and Brun*, 1984; *Vendeville et al.*, 1987; *Merle and Vendeville*, 1995). We use silicone to model the weak layer in the substratum. Silicone is a Newtonian fluid with a viscosity of about 10^4 Pa s. It is commonly used to model the low-viscosity strata of sedimentary sections [*Cobbold*, 1993].

The ratio between the height of our models and of real volcanoes (H^*) is about 1.6×10^{-5} (1 cm represents 600 m), whereas the ratio between the densities in experiments and nature (ρ^*) is about 0.56. Since gravity is the same both in experiments and reality ($g^*=1$), then, to a first order of approximation, the stress ratio may be calculated from

$$\sigma^* = \rho^* g^* H^* \approx 10^{-5} . \quad (14)$$

This means that our experimental models are about 10^5 times weaker than real volcanoes.

Experimental Procedure

During the experiments, the rate of spreading decreases exponentially with time and most of the deformation is achieved in about 10 hours. The progressive evolution of model deformation is recorded by overhead time-lapse photography of the model top surface. After the end of each experiment, models are serially sectioned and photographed.

Four different types of experiments are described: the first is a sand cone with a substratum that has no weak ductile layer (only the brittle layer is present), the second is a cone with a substratum composed of a brittle layer overlying a weak ductile layer, the third is like the second but is buttressed along two edges of the experimental box, and the fourth has only the ductile layer (no brittle layer is present).

Experimental Results

Substratum With a Brittle Layer Only

The first experiment has no silicone layer at the base of the substratum (experiment 0, see Table 3), equivalent to having a very thin silicone layer (that is, $\Pi_3 \rightarrow \infty$) of high viscosity. Whatever the thickness of the sand layer, no time

Table 3. Principal Characteristics of Representative Experiments Discussed in the Text

Experiment	Π_1	Π_2	Π_3	Π_4	Results
		Substratum With a Brittle Layer Only			
0	0.58	∞	∞	1	no deformation
		Substratum With a Brittle and a Ductile Layer			
1	0.58	0.4	4.5	1	sagging without deformation (very weak ductile layer)
2	0.58	0.3	0.75	1.5	spreading, 15-20 grabens
6	0.58	0.1	1	1	spreading, 8-10 grabens
7	0.58	0.4	4	1	no deformation
		Buffering Effect of Solid Boundaries			
3	0.58	0.3	1.1	1	four grabens in the unbuttressed direction only
		Substratum With a Ductile Layer Only			
8	0.58	0.02	0.2	1	spreading, 30-35 grabens

deformation of the free upper surface is recorded in the photographs. This result suggests that in the absence of a decollement zone, volcanic constructs should not spread. As already proposed by some authors [*Borgia et al.*, 1992; *McGovern and Solomon*, 1993], an essential requirement for spreading is the presence of a decollement zone (a weak layer) within the substratum of volcanoes. Even when considering the component of spreading related to the long-term deformation of the intrusive complexes [*Mc Donald*, 1965; *Borgia and Treves*, 1992; *Borgia*, 1994; *Clague and Denlinger*, 1994], the effect of the basal decollement remains an essential feature of the spreading process [*Borgia*, 1994]. However, it is emphasized that this statement about stability conditions results from experiments where no magma forces act upon the volcanic edifice.

Substratum With a Brittle and a Ductile Layer

By adding a weak ductile layer at the base of the model, two different kinematic evolutions may be observed; either subsidence of the sand cone without any deformation or failure of the cone leading to radial faults within the cone and folding and thrusting in the substratum surrounding the spreading cone.

In both cases, the silicone spreads radially under the load of the sand cone away from the center. In the second, however, the horizontal stress created by the viscous flow is sufficient to extend and tear apart the brittle substratum and the cone (Figure 2). The stretched brittle substratum under the analogue volcano shows both homogeneous stretching and boudinage (Figure 2d). The result is an increase in diameter of the sand cone, associated with radial paths of particles within the analogue volcano. Radial grabens (leaf graben) accommodate the concentric extension due to the radial displacement. The relief is rapidly smoothed as the cone spreads into a flat shield. A similar process was suggested by *Dieterich* [1988] to explain how the slopes of Hawaiian volcanoes are controlled by the frictional forces on the decollement between the volcanoes and the ocean crust.

Conjugate normal faults, accompanying the deformation of the sand cone, bound the grabens that dissect its upper surface. Grabens intersect toward the center of the cone producing on top a circular flat area. They also narrow toward the edge of the sand cone (Figures 1c and 2) identifying between them triangular "stable" horsts (wedge horsts). Serial cross sections show that conjugate faults join at the base of the model, that is, within the weak layer of silicone (Figures 1b and 2d). Small diapirs of silicone rise in the joining region forming the boudins of the stretched brittle subratum.

A concentric ridge develops around the sand cone (Figure 2). On cross sections, this ridge is an asymmetric fault-propagation anticline that verges away from the cone (Figures 1b and 2d). The thrust fault associated with the anticline roots horizontally at depth in the weak layer (decollement zone). The fold grows in part at the expense of the silicone layer, which thins beneath the load of the sand cone and thickens in the thrusting area.

Buffering Effect of Solid Boundaries

The symmetry of the deformation of the spreading sand cone is broken by the proximity of solid boundaries that may buttress the cone (Figure 3). Spreading does not occur toward a solid boundary if this is too close to the edge of the analogue volcano. The deformation is similar to the unbuttressed case but affects the unbuttressed sides of the model only (Figures 3a, 3b, and 3c). A consequence of the buttressing is then the generation of a small strike-slip component of displacement (not visible in Figure 3a) along the two faults that bound the spreading area. In nature, a buttressing effect could be produced by different rheological properties of the substratum and/or by preexisting topographic relief, such as a mountain range or another volcano.

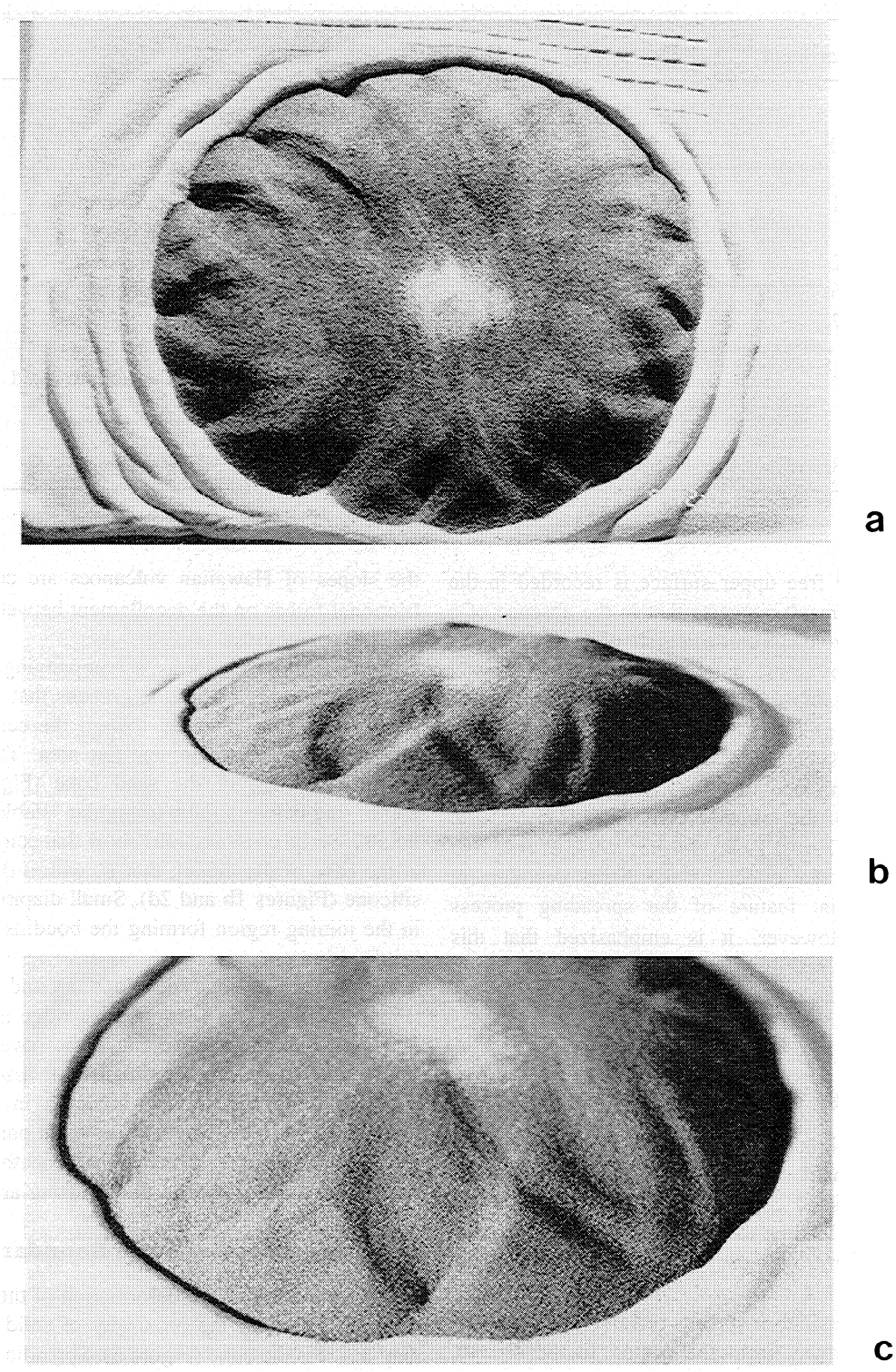

Figure 2. Upper free surface of spreading volcanoes showing the radial pattern of grabens and concentric thrust zones. (a) Experiment with Π_2=0.3, Π_3=0.75, Π_4=1.5 (experiment 2, diameter of the volcano is 24.5 cm). More than one concentric zone formed in this experiment. (b) Experiment with Π_2=0.1, Π_3=1, Π_4=1 (experiment 6, diameter of the deformed volcano is 22 cm). (c) Oblique view showing detail of the graben pattern in experiment 6. (d) Cross sections perpendicular to the central graben from experiment 6. Small diapirs of the silicone layer rise at the junction of conjugate normal faults. Layer parallel shortening in the substratum occurs at the edge of the analogue volcano. The uppermost horizontal layer of sand is added after deformation for technical convenience.

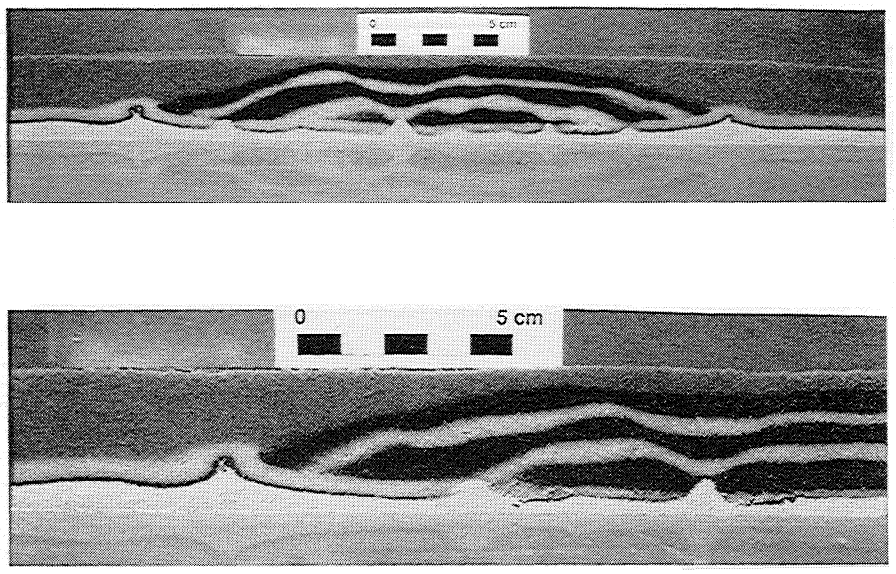

d

Figure 2. (continued)

Substratum With a Ductile Layer Only

Emplacing the sand cone directly onto the silicone layer (i.e., with no brittle horizon) leads to fast spreading of the sand cone that becomes a pancake-like edifice with a large number of grabens (Figure 4). Several generations of grabens superpose in time. A fold belt forms around the spreading cone revealing strong horizontal shortening associated with the radial displacement of the edge of the analogue volcano. In this case, the effect of the compression propagates far beyond the concentric fold belt at the base of the cone producing subsequent rings of isolated folds. The wavelength of these folds is probably a function of viscosity and surface tension of the silicone and might not mimic natural conditions.

A Natural Example: Etna Volcano

The evolution of the sand cone on weak substratum reflects the patterns of deformation that can be observed on actual volcanoes. In particular, three main features are directly comparable: (1) the summit horst-and-graben structure, (2) the basal deformation belt, and (3) the subvolcanic diapirs.

Figure 5a shows the summit of Etna volcano. This area is characterized by a large depression that is formed by erosion along two grabens trending ESE and N-S that intersect at one end [*Borgia et al.*, 1992]. As in the scaled experiments, the grabens narrow downhill and identify triangular "stable" horsts (Figure 5b). The faults that bound the graben show a strike-slip component especially close to the Tertiary mountain range, which buttresses the volcano to the north and to the west (A. Tibaldi et al., unpublished manuscript, 1995). A large fault-propagation anticline, verging away from the volcano, surrounds the unbuffered base [*Borgia et al.*, 1992]. Outcrops of clay beds along the basal anticline and along the Pernicana fault [*Romano*, 1992] (Figure 5b) could be outcrops of annular and radial diapirs respectively such as those in Figure 2d. Finally, we observe that Etna has a Π_3 between 0.1 and 1, is buttressed on two sides, and has at least four leaf grabens (Figure 5b); these observations compare well with those of the buttressed experiment (Table 3, experiment 3, and Figure 3c), where for a Π_3 of about 1 there is a similar number of grabens.

Discussion on the Dimensionless Numbers

The dimensionless numbers describe the dynamic evolution of the system. They vary with time depending on whether deformation takes place or not. For instance, during spreading, the dimensionless numbers Π_2 and Π_3 increase with time up to values that correspond to stable configurations. These final values tend to the values of experiments with no deformation. Π_3 is the dimensionless number that can show the largest variation in nature, from 0 to ∞, whereas other dimensionless numbers reveal little variation.

At the beginning of each experiment, the value of Π_1 is $\tan\Phi$=0.58, because the sand cone is made of granular material with angle of friction Φ which gives a slope angle of about 30°. During the experiment, Π_1 decreases with time and, at the end, will be the slopes of stable sand cones for any given substratum.

Π_2 is important because it gives the critical height (H) for a given thickness of the brittle substratum (D) above which the load of the analogue volcano is large enough to trigger deformation. In the experiments, this happens when Π_2 is less than 0.4. The deformation will increase Π_2 with time until it reaches a value close to 0.4. For values of Π_2 larger than about 0.4, the weight of the sand cone does not overcome the strength of the brittle substratum. Of course,

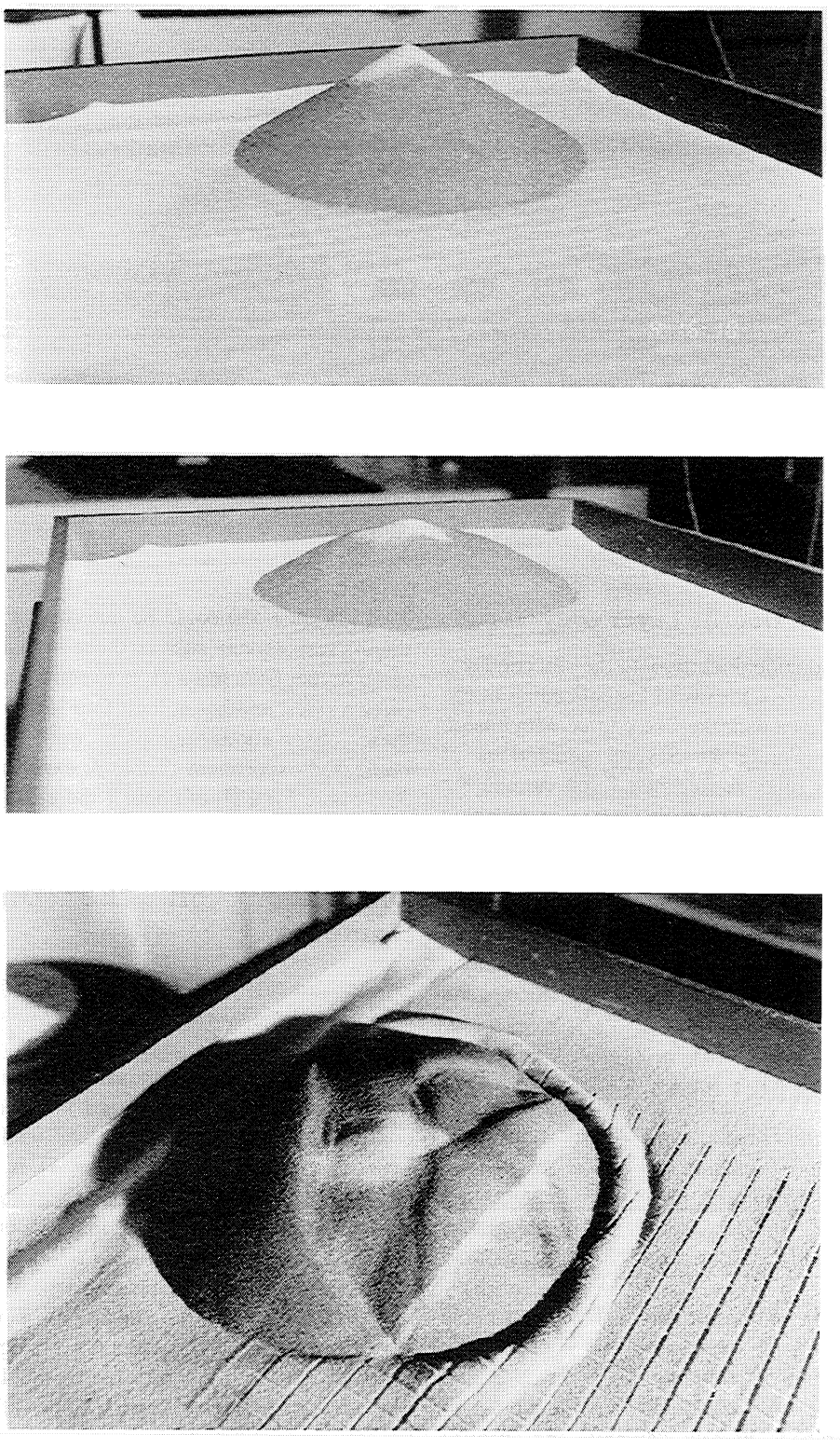

Figure 3. Oblique view of a spreading analogue volcano (Figures 3a, 3b, and 3c are experiment 3 with Π_2=0.3, Π_3=1.1, Π_4=1; width of the box is 50 cm). (a) Initial stage. (b) Smoothed relief due to the spreading process 2 hours after figure 3a. (c) Upper free surface at the end of the experiment (10 hours) showing four grabens in the analogue volcano and a concentric thrust zone around it. Displacements occurred in unbuttressed directions only. This pattern is remarkably similar to the one observed at Etna volcano (Figure 5).

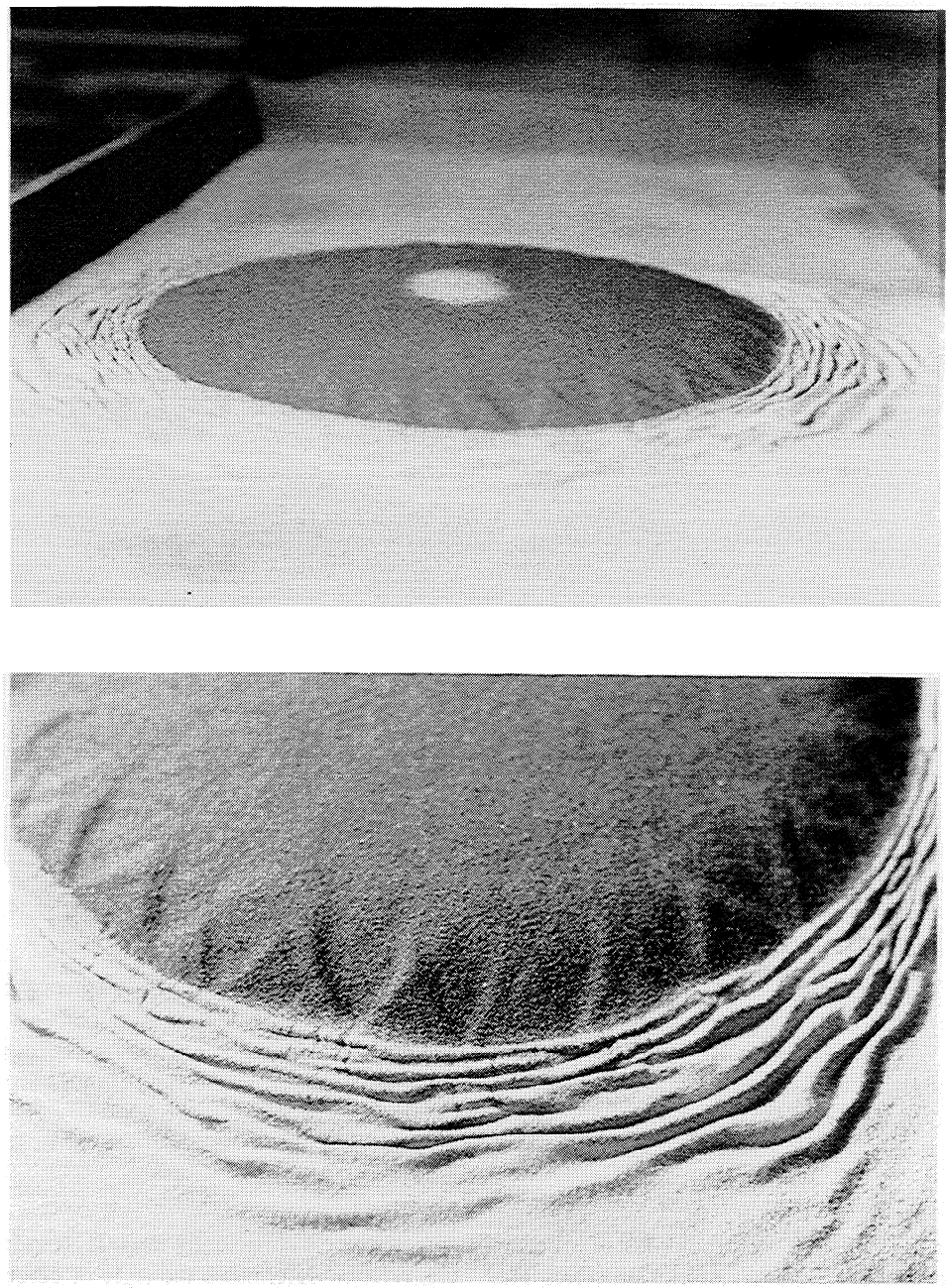

Figure 4. Oblique view and detail of experiment with Π_2=0.02, Π_3=0.2, Π_4=1 (experiment 8; width of the box is 50 cm) showing spreading of the cone into a pancake-like edifice and the fold belt around it.

this threshold value is also a function of the density ratio Π_4. The silicone flows radially outward below the brittle layer allowing only the sagging of this layer and of the sand cone, but not its fracture.

The brittle/ductile ratio (Π_3) is the dimensionless number that determines the style of deformation. It is the essential parameter that controls the two main evolutionary trends observed in the experiments: simple sagging of an undeformed cone versus failure of the cone. If $\Pi_3 >> 1$, there is a locking effect due to the strength of the substratum and no deformation occurs: the sand substratum either remains stable, if there is a high viscosity (low Π_5) or no weak layer, or sags under the load of the cone as the silicone flows away from underneath (Figure 6a). Two experiments conducted with a $\Pi_3 = \sim 4$ show either sagging with a low-viscosity layer (7×10^3 Pa s, Figure 7, experiment 7) or stability with a higher viscosity (2×10^4 Pa s).

For Π_3 around 1, one single concentric ridge develops around the spreading analogue volcano. This ridge is the result of folding and thrusting, which verges away from the cone (Figure 6b). For $\Pi_3 << 1$, a fold belt develops around the spreading cone (Figure 6c). Folds are very tight, and the weak layer may crop out at the surface, breaking up the

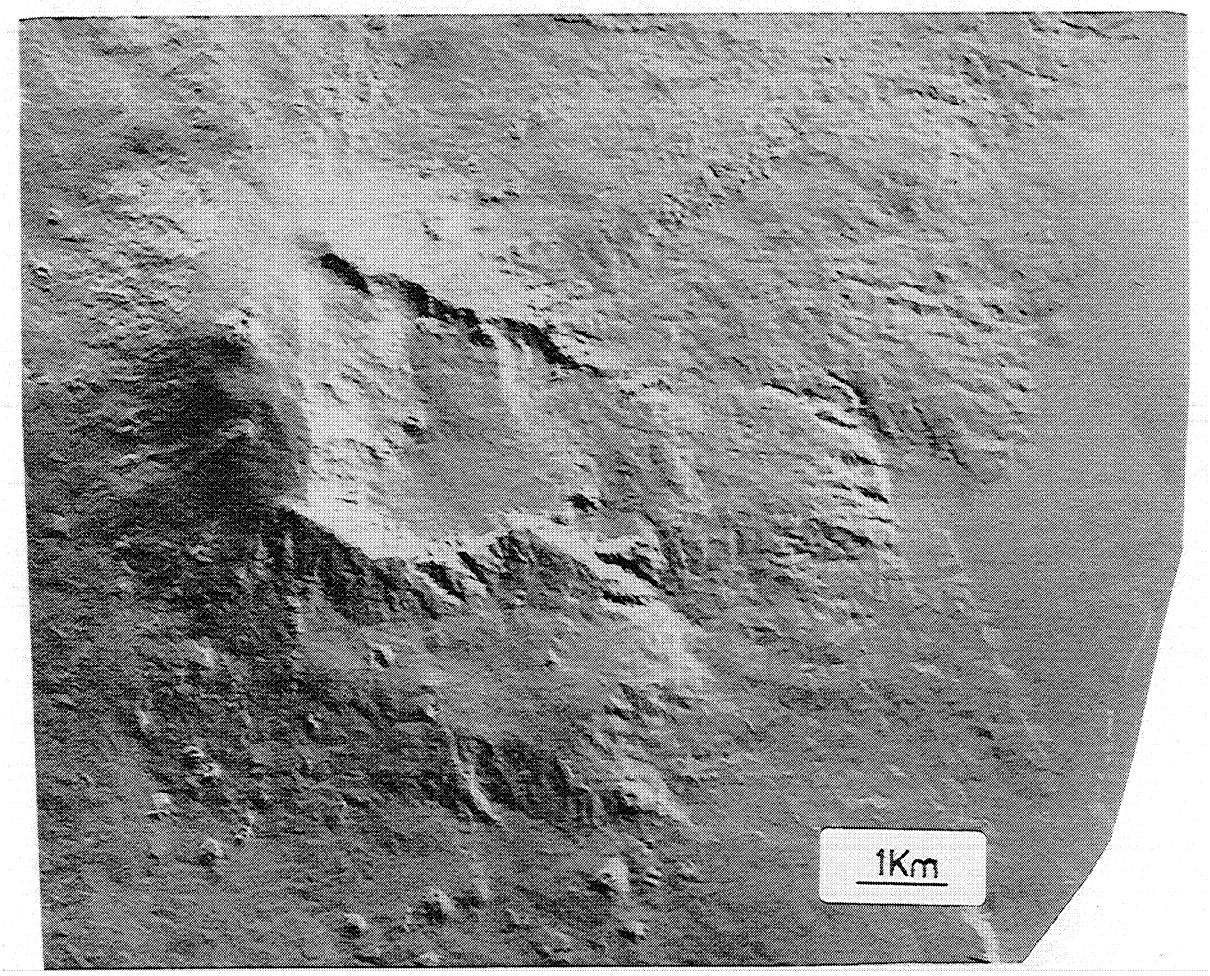

Figure 5a. Digital elevation model of the summit of Etna volcano. Note the large depression (Valle del Bove), east of the summit, though to have formed by erosion along two intersecting grabens, striking N-S and WNW-ESE; the faults that bound to the west the north striking graben and to the north the ESE striking graben are also visible; the other bounding faults are observed in the field (Figure 5b); image processed by G. Macedonio and M.T. Pareschi at the University of Pisa.

thin brittle upper layer. These local outcrops of silicone, due to strong horizontal shortening, form structures that mimic the rise of diapirs from low-density horizons in sedimentary sections. The number of grabens which develop within the spreading cone is also dependent on the value of Π_3. A high Π_3 (about 3) leads to the formation of six to seven grabens, whereas a low value (1 or less) leads to a larger number of grabens (Figures 2a-2c, 3c, and 4). Just as the other numbers, Π_3 increases with time reaching values close to those of experiments with stable configuration.

The relation between Π_1 and Π_3 controls the dynamic evolution of volcanoes. For instance, whereas the slope of the cone (Π_1) decreases with time, the brittle/ductile ratio of the substratum (Π_3) changes slightly. This relation reveals the evolution of a cone from an unstable condition, which initiates spreading, to a stable one where spreading has stopped (Figure 7). A spreading boundary separates volcanoes that will never spread from those that may spread given a sufficiently large Π_1 (Figure 7). In addition, this relation determines the style of deformation.

In nature, however, spreading may be continuous in time, never coming to halt, because a volcanic edifice may grow by the emplacement of both intrusions and surficial products. They increase the value of Π_1 forcing the volcano to become unstable [*Dieterich*, 1988].

The effect of the weight of the volcano on the substratum can be estimated from the density ratio Π_4. Increasing Π_4 (from 1 to 1.5) has the same effect as decreasing Π_3. That is, the weight of the volcano is a key parameter to overcome the strength of the brittle substratum. For example, keeping Π_3 around 1 and increasing Π_4 to 1.5 leads to the growth of a fold belt around the analogue volcano and to the formation of a larger number of grabens that are usually oberved for a smaller value of Π_3 (compare Figures 2a and 3c).

Π_5 constrains the rate at which deformation occurs. In the experiments, Π_5 is mainly an inverse function of the

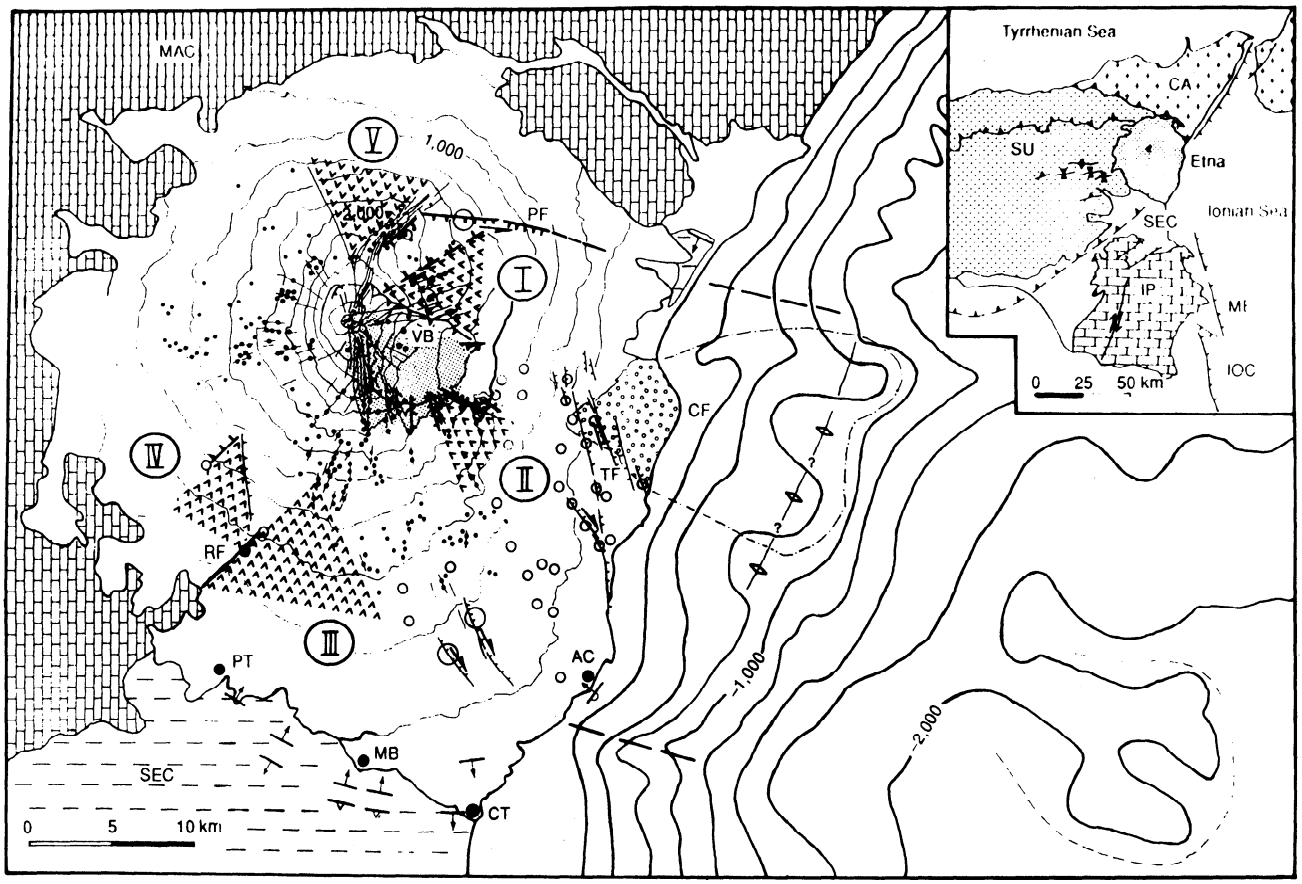

Figure 5b. Map of Etna [after *Borgia et al*, 1992] with major inferred wedge-like "stable" horsts (I-IV and v pattern). These horsts form topographic highs that are almost devoided of volvanic and seismic activity. The northern fault of horst I is from *del Negro and Napoli* [1995]. West of horst V is the stable sector of the volcano. Erosion along intersecting grabens formed the Valle del Bove (VB) and the Chiancone fanglomerate (CF). A set of fault-propagation folds occurs around the base of the volcano south of Paterno (PT) and Misterbianco (MB), north of Catania (CT) and east of Aci Castello (AC). The Pernicana (PF [*Borgia et al.*, 1992]) and the Ragalna (RF *[Rust and Neri*, 1996]) trantensional faults and the summit rift zones limit the sector of the volcano that is buffered by the Maghrebian-Appenine chain (MAC) from the other spreading sectors. The MAC is composed of the Calabrian Arc (CA) and the Sicilide units (SU). South of the chain is the Iblean Plateau (IP) covered by the sub-Etnean clays (SEC), which form the weak substratum. Large normal faults, called "Timpe" (TF), cut the eastern sector of the volcano and seem to follow inland the Malta escarpment (ME), that is the western border of the Ionian ocean crust (IOC).

viscosity of the silicone layer. A low viscosity makes Π_5 large and facilitates spreading. In nature, however, Π_5 has a different meaning. Since the height of the volcano increases with time as the volcano grows, the increase of Π_5 shows the transition from a stable to a spreading cone.

If we accept that the similarity conditions are satisfied, then from (5), we obtain

$$t = \frac{\Pi_5}{\rho g H}\mu \qquad (15)$$

where Π_5 is obtained from the experiments.

Thus a first-order calculation indicates that in actual volcanoes the timescale for deformation is directly proportional to the viscosity of the weak layer, because the denominator of (15), $\rho g H$, varies at most by 1 order of magnitude for the whole range of volcanic edifices. Clearly, for very small viscosities (10^{15} Pa s) the layer is so weak that it cannot sustain the erupted volcanics long enough ($>10^3$ years) for an edifice to grow. On the other hand, for much larger viscosities (10^{19} Pa s) the time of deformation ($>10^6$ years) becomes longer than the lifespan of volcanoes [*Shaw*, 1987], and erosion will smooth the topographic relief well before spreading becomes significant.

In conclusion, the interaction of dimensionless numbers controlling the spreading process is complex. A "rule of thumb," however, is that the spreading rate is high for a small Π_2 and Π_3 and a large Π_4 and Π_5.

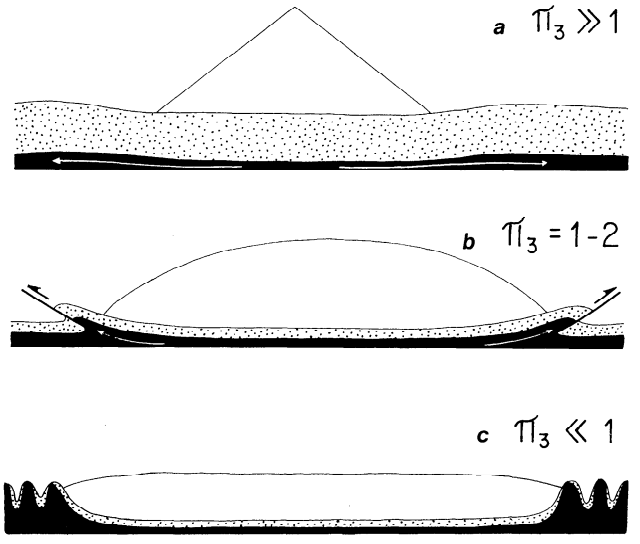

Figure 6. The three deformation styles observed in experiments as a function of Π_3. (a) $\Pi_3>>1$, sagging of the undeformed cone; (b) $\Pi_3=1$-2, formation of a shield edifice with a concentric ridge; and (c) $\Pi_3<<1$, formation of a pancake edifice with a fold belt.

Conclusions

The experiments described above indicate that spreading induced by volcanic loading is strongly controlled by geometry and type of substratum. In particular, spreading takes place only if (1) there is a weak layer in the substratum, (2) the thickness of the brittle layer above the weak layer is relatively thin, and (3) the volcano is not buttressed on all sides.

In continental environments, volcanic edifices may overlie sedimentary basins which comprise evaporite horizons (Aucamahuida volcano in Argentina [*Digregorio and Uliana*, 1980]), marls, clays (Etna volcano [*Borgia et al.*, 1992]), deeply altered volcanic rocks (Poas volcano in Costa Rica [*Borgia et al.*, 1990]), or incompetent shales. Therefore, on continental volcanoes, spreading occurs if the brittle layer in the substratum is thin and underlain by low-viscosity rocks and if the edifice is unbuttressed for a relatively large sector. In oceanic environments, the deposits emplaced by oceanic sedimentation (of clay, silt, and marls) or by mass wasting from oceanic volcanoes may play the role of the low-viscosity decollement zone, as is the case in Hawaii [*Nakamura*, 1980].

The three conditions stated above are necessary but not sufficient for spreading. The requirements for spreading are given by dimensionless numbers which fulfill the similarity between nature and experiments. Π_2, which is the ratio between the thickness of the brittle substratum and the height of the volcano, should be less than 0.4, and Π_3, which corresponds to the brittle/ductile ratio in the substratum, should be less than 4 for collapse to start. Π_2 and Π_3 values in excess of 0.4 and 4, respectively, correspond to volcanic constructs showing stable configuration. Once the collapse of the edifice starts, these two dimensionless numbers increase, and the deformation lasts until Π values reach those of a stable configuration. However, Π_3 is the key parameter as a very large value (around 10) prevents the spreading process even when Π_2 is less than 0.4. Thus our experiments emphasize that the Π_3 dimensionless number determines whether the spreading process takes place or not.

Π_3 is also the parameter which controls the style of deformation. Three principal patterns of deformation can be observed from high to low values of Π_3: (1) sagging of the volcano without any deformation, (2) spreading of the volcano with the growth of concentric ridges in the substratum around the resulting shield edifice, and (3) spreading of the volcano with the growth of a concentric fold and thrust belt around the resulting pancake edifice. In the last two cases, the deformation within the volcano leads to the formation of a number of intersecting radial leaf grabens and wedge horsts that is inversely proportional to Π_3.

We find it to be remarkable that some essential features of volcanoes like the ones described above are modeled correctly by such simple experiments. To the best of our knowledge, leaf grabens and wedge horsts were not described before on volcanoes, not was their relevance in the dynamics of volcanic deformation recognized. A future challenge for field geologists is to produce detailed descriptions of the geometry, kinematics, and dynamics of such structures.

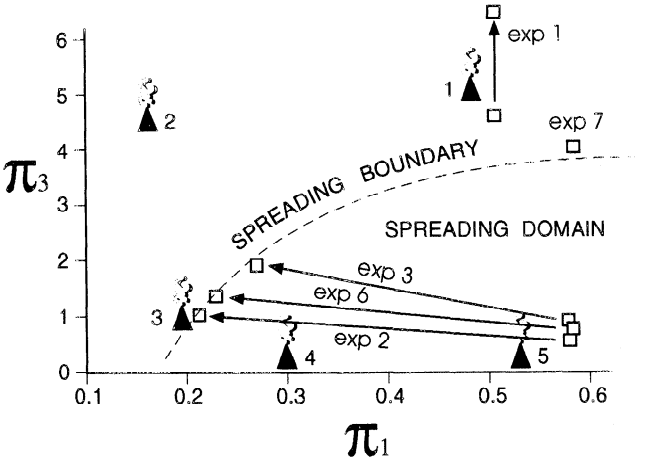

Figure 7. Π_1 versus Π_3 graph showing the boundary between spreading and nonspreading domains. Time evolution for dimensionless numbers in experiments reveal deformation paths toward the nonspreading boundary. Data from real volcanoes plot in the different fields according if they are actively spreading (4, Etna and 5, Concepcion), already spread to a stable configuration (3, Poas) and nonspreading (2, Kilimanjaro, and 1, Arenal). Experiment 7 corresponds to sagging without deformation as a result of flow of a very low-viscosity layer (7×10^3 Pa s).

Acknowledgments. G. Macedonio and M.T. Pareschi provided the digital elevation model of Etna. Financial support to this work was provided by the French PNRN project (INSU-CNRS, project RV03), ING, GNV-CNR grant 94.01625.PF62, EC grant EV5V-CT92-0170, and NERC small grants. Experiments were conducted at the experimental laboratory of Geosciences Rennes, the University of Rennes, France. We thank Maurizio Battaglia for discussing the paper. We are greatly indebted to P. Delaney, P. J. McGovern, D.F. McTigue, and P. Wessel for their constructive reviews of the manuscript.

References

Argnani, A.C., C. Savelli, and A. Borgia, Structure and dynamics of Marsili seamount (Tyrrhenian backarc basin) (abstract), *Eos Trans. AGU, 74*(43), Fall Meet. Suppl., 646, 1993.

Borgia, A., Evoluzione strutturale dei vulcani a scudo terrestri e marziani, paper presented at 75th Congresso Nazionale, Soc. Geol. Ital., Milano, 1990.

Borgia, A., Dynamic basis for volcanic spreading, *J. Geophys. Res., 99*, 17,791-17,804, 1994.

Borgia, A., and B. Treves, Volcanic plates overriding the ocean crust: structure and dynamics of Hawaiian volcanoes, *Ophiolites and Their Modern Analogues*, edited by M.L. Parson, J.B. Murton, and P. Browning, *Geol. Soc. Spec. Publ. London, 60*, 277-299, 1992.

Borgia, A., J. Burr, W. Montero, L.D. Morales, and G.E. Alvarado, Fault propagation folds induced by gravitational failure and slumping of the Central Costa Rica Volcanic Range: Implications for large terrestrial and Martian volcanic edifices, *J. Geophys. Res., 95*, 14,357-14,382, 1990.

Borgia, A., L. Ferrari, and G. Pasquare, Importance of gravitational spreading in the tectonic and volcanic evolution of Mount Etna, *Nature, 357*, 231-235, 1992.

Clague, D.A., and R.P. Denlinger, Role of olivine cumulates in destabilizing the flanks of Hawaiian volcanoes, *Bull. Volcanol., 56*, 425-434, 1994.

Cobbold, P.R. (Ed.), New insight into salt tectonics, *Tectonophysics*, 228(3/4), 1993.

Delaney, P., You can pile it only so high, *Nature, 357*, 194-196, 1992.

Del Negro, C., and R. Napoli, Indagine Magnetica nell'alto versante orientale dell'Etna. Paper presented at La dinamica del versante orientale Etneo con particolare riferimento al ruolo del sistema Faglia Pernicana, Rift di NE, Cons. Naz. delle Ric., Catania, Italy, April 21, 1995.

Dieterich, J.H., Growth and persistence of Hawaiian volcanic rift zones, *J. Geophys. Res., 93*, 4258-4270, 1988.

Digregorio, J.H., and M.A. Uliana, Cuenca Neuquina, *Secundo Simposio de Geologia Regional Argentina*, vol. II, pp. 985-1032, Sociedad Geologica Argentina, Buenos Aires, 1980.

Faugère, E., and J.P. Brun, Modélisation expérimentale de la distention continentale, *C. R. Acad. Sci., 299*, 365-370, 1984.

Hubbert, M.K., Theory of scale models as applied to the study of geologic structures, *Geol. Soc. Am. Bull., 48*, 1459-1520, 1937.

Hubbert, M.K., and W.W. Rubey, Role of fluid pressure in mechanics of overthrust faulting, I. mechanics of fluid-filled porous solids and its application to overthrust faulting, *Geol. Soc. Am. Bull., 70*, 115-166, 1959.

Kerr, A., Volcanoes with bad hearts are tumbling down all over, *Science, 264*, 660, 1994.

Mc Donald, G. A., Hawaiian calderas, *Pac. Sci., 19*, 320-334, 1965.

McGovern, P.J., and S.C. Solomon, State of stress, faulting, and eruption characteristics of large volcanoes on Mars, *J. Geophys. Res., 98*, 23,953-23,579, 1993.

Merle, O., and B.C. Vendeville, Experimental modelling of thin-skinned shortening around magmatic intrusions, *Bull. Volcanol., 57*, 33-43, 1995.

Merle, O., R.P. Nickelsen, G.H. Davis, and P. Gourlay, Relation of thin-skinned thrusting of Colorado Plateau strata in southwestern Utah to Cenozoic magmatism, *Geol. Soc. Am. Bull., 105*, 387-398, 1993.

Nakamura, K., Why do long rift zones develop in Hawaian volcanoes-A possible role of thick oceanic sediments, *Bull. Geol. Soc. Jpn.,25*, 255-267, 1980.

Pasquarè, G., L. Farrari and A. Borgia, Rifting and spreading of the Cappadocia volcanic plateau, Turkey (abstract), *Eos Trans. AGU, 74* (43), Fall Meet. Suppl., 647, 1993.

Ramberg, H., *Gravity, Deformation and the Earth's Crust, 452 pp.*, Academic, San Diego, Calif., 1981.

Romano, R., Mt Etna: Carta naturalistica e turistica, Florence, Italy, 1992.

Rust, D.G., and M. Neri, The boundaries of large scale collapse on the flanks of Mt Etna, in *Volcano Instability on the Earth and other Planets*, edited by W. C. Mc Guire, A. P. Jones, and J. Neuberg, *Spec. Publ. Geol. Soc. London, 110*, 193-208, 1996.

Shaw, H.R., Uniqueness of volcanic systems, in *Volcanism in Hawaii, U.S. Geol. Surv. Prof. Pap., 1350*, 1357-1394, 1987.

van Bemellen, R.W., *The Geology of Indonesia: General Geology of Indonesia and Adjacent Archipelagoes*, Gov. Print. Off., The Hague, Netherlands, 1949.

van Wyk de Vries, B., Spreading at Concepcion volcano, Nicaragua (abstract), *Eos Trans. AGU, 74*(43), Fall Meet. Suppl., 646, 1993.

Vendeville, B., P.R. Cobbold, P. Davy, J.P. Brun, and P. Choukroune, Physical models of extensional tectonics at various scales, in *Continental Extensional Tectonics*, edited by M.P. Coward, M.F. Dewey, and P.L. Hancock, *Spec. Publ. Geol Soc. London, 28*, 95-107, 1987.

A. Borgia, Instituto Nazionale de Geofisica, via di Vigna Murata 605, 00143 Rome, Italy. (e-mail: Borgia@in8800.ingrm.it)

O. Merle, Département des Sciences de la Terre, 5 rue Kessler, 63038 Clermont Ferrand Cedex, France. (e-mail: merle@opgc.univ-bpclermont.fr)

(Received January 10, 1995; revised November 13, 1995;
accepted November 21, 1995.)